scientific reports

OPEN

Tailoring elastic and inelastic collisions of relativistic antiferromagnetic domain walls

Rubén M. Otxoa[1,2✉], Gen Tatara[3], Pierre E. Roy[1] & Oksana Chubykalo-Fesenko[4✉]

Soliton-based computing relies on their unique properties for transporting energy and emerging intact from head-on collisions. Magnetic domain walls are often referred to as solitons disregarding the strict mathematical definition requiring the above scattering property. Here we demonstrate the conditions of elastic and inelastic scattering for spin–orbit torque-induced dynamics of relativistic domain walls on the technologically relevant Mn_2Au antiferromagnetic material. We show that even domain walls with opposite winding numbers can experience elastic scattering and we present the corresponding phase diagram as a function of the spin–orbit field strength and duration. The elastic collision requires minimum domain walls speed, which we explain assuming an attractive potential created by domain wall pair. On the contrary, when the domain walls move at lower speeds, their collision is inelastic and results in a dispersing breather. Our findings will be important for the development of soliton-based computing using antiferromagnetic spintronics and we discuss their prospects for building NOT and XOR gates.

As particle-like highly localized objects, solitons can carry and exchange information, which make them unique entities for example, for unconventional computation[1,2]. Robustness to perturbations and very importantly to collisions is an essential ingredient to build soliton-based nanoelectronics. Soliton-based information processing is typically discussed in relation to their technological applications to nonlinear optics[3,4], other possibilities such as semiconductor waveguides[5,6] or Bose–Einstein condensates also exist[7–9]. Optical solitons are very localised and fast (typical temporal width corresponding to femto-picosecond timescale) and thus can potentially be used in ultrafast computing and electronics.

On the other hand, antiferromagnetic spintronics is currently attracting huge attention due to its energy efficiency, high speed, abundance of materials and invisibility to external magnetic fields[10–12]. Importantly, anti-ferromagnetic domain walls have solitonic nature and are not only ultrafast[13] (with velocities up to 40 km/s) but also relativistic and thus contract their length allowing their "charging" by exchange energy and its consequent transport[14–16]. The "discharge" takes place when two domain walls with opposite topological charges collide[13,14]. They can also exhibit multi-cascading processes useful for transporting information from one collision to the next[13]. Being close to solitons and related to the well-known sigma-model[17–19], antiferromagnetic domain walls of course do not obey the main property of mathematical solitons in exactly integrable systems which state that two (or more) wave packets when collide maintain their shapes. As we show in this article, these conditions, however, can be controlled by strength and duration of current pulses, making them very useful candidates for soliton-based applications.

In nano-magnetism a soliton is interpreted as a spatially localised perturbation whose stability is provided by the magnetisation field structure[20–22]. Therefore, the elastic collision requirement is relaxed when referring to domain walls (DW), vortices, skyrmions, etc. as solitons. A more accurate way to coin magnetic domain wall is *kink* which connects two ground states but still allows for two objects to annihilate. However, for the recombina-tion to occur one needs to attend for the topological character of the two magnetic textures[20,23]. Distinct topologi-cal textures are characterised by different winding number, w, which counts the number of times the magnetisa-tion is wrapped onto itself[22]. The winding number density at each point in time t, is $w(x,t) = -\nabla_x \phi(x,t)$, with the total winding number (topological charge) being $\frac{1}{2\pi} \int w(x,t)dx$, which for a 180° domain wall takes values $\pm\frac{1}{2}$. Here $\phi(x,t)$ is the in-plane angle of the spin at location x at time t of the spin-configuration along the one

[1]Hitachi Cambridge Laboratory, J. J. Thomson Avenue, Cambridge CB3 0HE, UK. [2]Donostia International Physics Center, Paseo Manuel de Lardizabal 4, 20018 San Sebastián, Spain. [3]RIKEN Center for Emergent Matter Science (CEMS) and RIKEN Cluster for Pioneering Research (CPR), 2-1 Hirosawa, Wako, Saitama 351-0198, Japan. [4]Instituto de Ciencia de Materiales de Madri, CSIC, Cantoblanco, 28049 Madrid, Spain. ✉email: ro274@cam.ac.uk; oksana@icmm.csic.es

dimensional infinite line. Magnetic textures whose winding number (WN) do not change in time are usually called topological solitons[20,23]. Topological character of domain walls is very advantageous from the point of view of applications such as soliton-based computing, since it conveys them the necessary stability against perturbations and simple particle-like behavior.

Strictly speaking a magnetic topological soliton (TMS) requires its WN to be a constant of motion. However, magnetic textures instabilities such us Walker-Breakdown (WB) for domain walls[24] or vortex core reversal for vortices[25] lead to a continuous change of the WN. Moreover, applications of sufficiently strong magnetic fields annihilate any magnetic texture. Thus, magnetic structures can be referred as topological magnetic solitons only in some limited sense. Here after, we focus on dynamical regimes far from these instabilities, i.e. when the topological charge is conserved. In this case, two magnetic textures with opposite winding number can annihilate each other to generate uniform ground state as both spin arrangements belong to the same topological class[22] leading to inelastic collision. However, if both domain walls have the same winding number, the recombination is not allowed as there is no continuous deformation to reach the uniform state. Therefore, at first glance, one would expect that elastic collision property would be reserved only for textures with the same winding number elevating their fundamental character to topological solitons. This has been confirmed recently experimentally[26,27] and numerically[28–30] for ferromagnetic textures. The scenario where the collision occurs between two magnetic textures with opposite winding number has always shown a non-soliton character both in experiment[31,32] and simulations so far[30,33] as a DW recombination was observed. The question we address in this work is whether recombination phenomenon between magnetic textures with opposite winding number can be avoided and if so under what specific conditions. Anticipating our findings, the proper tailoring of the current pulse duration in antiferromagnetic materials such as Mn_2Au can allow the control over elastic and inelastic scattering. The key property is the velocity achieved by domain walls during the current application. This provides some of the necessary ingredients for soliton-based computing and we discuss the possibilities to create NOT and XOR gates for possible nanoelectronics applications.

Results

In this work, we demonstrate that antiferromagnetic (AF) DWs with opposite WN can preserve their integrity after a head on collision moving above certain critical speed. To elucidate the control over the elastic scattering of antiferromagnetic domain walls (AF DWs), we use large-scale atomistic spin modelling of a layered antiferromagnet Mn_2Au. We consider that Mn_2Au is arranged in an ultra-thin stripe so that DW would have a one-dimensional propagation. In order to induce magnetisation dynamics in Mn_2Au, we make use of the predicted staggered field-like torque in such crystal structures, where the effective magnetic field resulting from a staggered-induced spin-density, H_{so}, possesses opposite signs at each sub-lattice and gives rise to a spin–orbit torque[34]. For the description of the atomistic model see Methods section. The DW mobility in Mn_2Au has been reported elsewhere[13,14,35]. The maximum AF DW speed, v_m can be obtained from the magnon dispersion relation and direct modelling and is circa 43.3 km/s for Mn_2Au[13].

In the continuum approximation and taking into account the relative values of anisotropy parameters (see Methods) one can obtain an equation for the in-plane component of the magnetisation Neel vector of the following form[35]

$$\frac{1}{v_m^2}\ddot{\varphi} - (\partial_x^2\varphi) + \frac{1}{2\Delta_0^2}\sin 2\varphi = -h\sin\varphi - \eta\dot{\varphi}, \tag{1}$$

Here $\Delta_0 = \sqrt{a/(8K_{2||})}$ stands for the DW width at rest, $h = 8\gamma\hbar H_{so}/a$ denotes the reduced scalar spin–orbit (SO) field related to the applied current, $\eta = 8\alpha\hbar/a$ describes the DW dissipation, $a = a_0^2(\mathscr{J}_3 + |\mathscr{J}_1|/2)$, where $\mathscr{J}_1$ and $\mathscr{J}_3$ are in-plane exchange parameters, $K_{2||}$ is an in-plane anisotropy (see Methods), a_0 is the lattice parameter, γ represents the gyromagnetic ratio, α is the Gilbert damping parameter and $\hbar$ is the reduced Planck constant. The l.h.s. of Eq. (1) is the famous exactly integrable sine-Gordon equation. Its soliton (kink) solution $\varphi = 2\arctan\exp[(x - vt)/\Delta]$ describes the AF DW having velocity v and velocity-dependent width $\Delta = \Delta_0\sqrt{1 - v^2/v_m^2}$. Note that it is also solution of a complete Eq. (1) provided that the r.h.s is zero, i.e. AF DW moves with a stationary velocity $v = (\gamma/\alpha)H_{so}\Delta$. Thus, AFDW has solitonic nature in the sense that it propagates without changing the form but only moving at a stationary velocity, i.e. when the energy input provided by the external current is compensated by the dissipation.

When two solitons of any integrable equation collide, they form a breather. The breather is not a solution of Eq. (1) and thus, a priory one cannot expect that AF DWs emerge intact from the collision. In the condition when topological charge is conserved and when two AF DWs have the same topological charge, this is indeed the outcome of the collision. When the two topological charges are opposite, as we will see later in complete simulations, two scenarios are possible attending to the duration of the driving mechanism, as illustrated schematically in Fig. 1. First, when the SO-field is present for long time, and the collision occurs, the Zeeman energy prevents the DWs to separate as the magnetisation orientation in between the DWs is polarised opposite to the SO-field. The resulting bound state is dispersing in time (Fig. 1a). In the second case, one can switch off the field at the right moment. Provided that the damping is small (which is indeed the case for magnetic systems) one can expect to find conditions that the resulting breather will not disperse before separating into two kinks (AF DWs).

We now present direct atomistic spin modelling results of AF DW dynamics under applied current producing SO-field based on Mn_2Au complete spin Hamiltonian (see Methods). Figure 2a–c shows the spatio-temporal evolution of magnetic configuration of a system with two DWs (having opposite winding numbers) colliding under application of H_{so}= 60 mT that is turned off at different instances. Figure 2a, shows the case where an inelastic collision is observed resulting in the breather dispersion. The reason for this is that the H_{so} has not been switched off after the collision and the associated Zeeman energy prevents AF DWs to separate as the region in
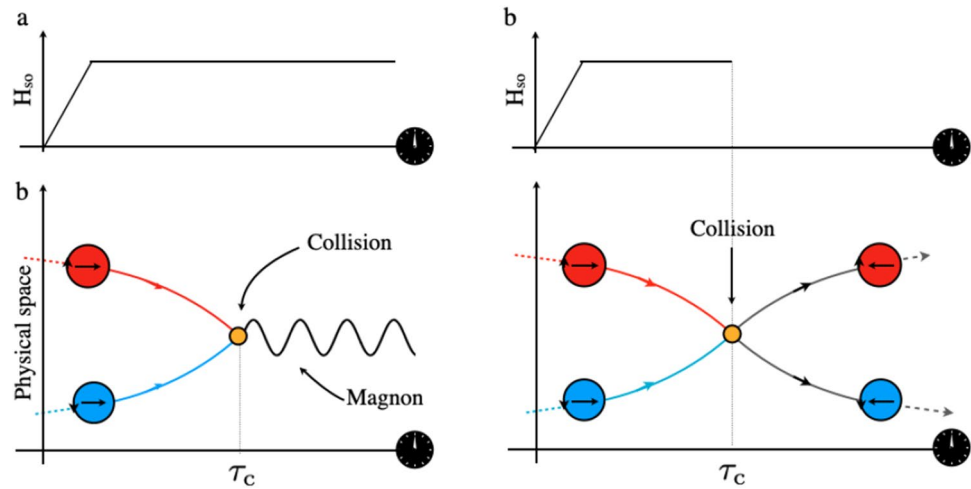
Figure 1. (**a**) Schematic illustration of two magnetic textures with opposite winding number driven by a SO-field which collide while the SO-field is present. In such a condition the inelastic collision gives rise to the excitation of breather. (**b**) Schematic illustration of two magnetic textures with opposite winding number driven by a SO-field which collide elastically in the absence of the SO-field. Each DW preserves its winding number after the collision however, there is a 180° phase-shift in the DW's internal spins.

between the two DWs have the opposite polarisation to H_{so}. However, if the SO-field is switched off when the collision occurs (for 60 mT at the time moment around 20.1 ps), then an elastic collision takes place, see Fig. 2b. We observe a discontinuity in the trajectory of each DW at the moment of the collision and the reappearance of the DW after they *tunnel* through each other. Importantly, it is observed that while the winding number is preserved through the entire collision process, there has been a 180° phase shift for the DW internal spins for both DWs, i.e. kink has become and anti-kink. The third possible scenario Fig. 2c results when the two DWs elastically collide but the distance between them is within the exchange interaction range to observe a recombination in the simulation time-window. The emergence of this breather-like excitation is due to the excess of kinetic energy carried by each DW involved in the collision. Note that, as expected, the resulting breather frequency is monochromatic and independent on the previously applied SO-field. Figure 2d presents the phase diagram with the possible outcomes observed depending on the magnitude of the SO-field and its duration. The smallest SO-field at which we observe soliton-like collision is 22 mT showing inelastic collision at 20 mT for for all investigated SO-field duration times.

From now on wards, we refer to AF DW of a given winding number as particle (p) and to that with opposite winding number as anti-particle (ap) indistinctly. Hence, one could interpret that each p (ap) behaves as an attractor for its ap (p). For an elastic collision to occur, p(ap) should escape from this potential, i.e. its kinetic energy, K_p must be larger than the attractive potential, V_{ap} provided by its own anti-particle. This potential at a given instant, t is given by the attractive exchange interaction between the two DWs with opposite winding number (see Appendix) and corresponds to

$$E_{\text{p-ap}} = 4A\left(x_p - x_{ap}\right)\cosh\left(\frac{x_p - x_{ap}}{\Delta}\right), \tag{2}$$

where x_p and x_{ap} represent the particle and anti-particle position with respect to an external and inertial observer. For sake of simplicity, we will locate the observer at the antiparticle such that $x_{ap}=0$. Note that this picture assumes that the breather is separated into two "kinks" which is valid when $|x_p - x_{ap}| \gg 4\ln(v/v_m)$. For domain walls moving with velocities close to that of the "light" $c = v_m$, this condition is very loose. Hence, we only need to calculate the DW mass[36–38] in order to obtain the kinetic energy, K_p

$$K_p = \frac{1}{2}m_p v^2 = \frac{1}{2}\frac{\hbar^2 N}{K_{2\perp}}\frac{v^2}{\Delta^2} \tag{3}$$

where $N = \pi\Delta/a_0$ is the number of spins that conform the DW and $K_{2\perp}$ is the second order perpendicular anisotropy, see Methods.

We consider that the particle has escaped the anti-particle potential when it is at least at a distance of DW width from the anti-particle, i.e. $x_p = \Delta$ giving the escape velocity

$$v_e = \left(\frac{32\pi\cosh(1)A\delta K_\perp}{h^2}\right)^{\frac{1}{2}}\Delta \equiv \xi\Delta(v_e). \tag{4}$$
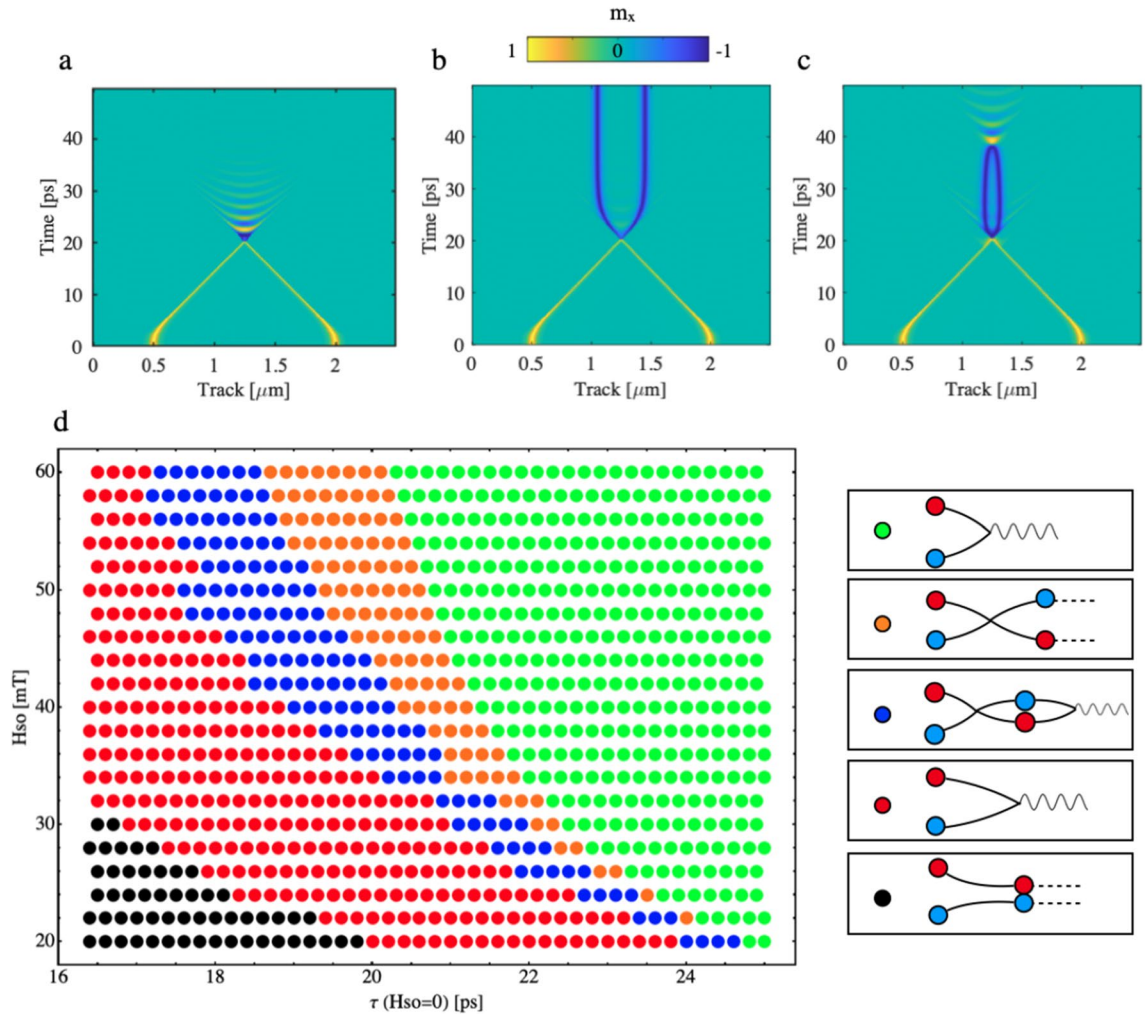
Figure 2. (**a**) Spatio-temporal evolution of the s_x component of the magnetisation when the SO-field is kept on during the entire simulation. Recombination event occurs and as a result there is a breather. (**b**) Spatio-temporal evolution of the s_x component of the magnetisation when the SO-field is turned off when the collision occurs. The two DWs behave as soliton appearing after the collision with the same winding number but with a 180° phase shift in its internal spins. (**c**) Spatio-temporal evolution of the s_x component of the magnetisation when the SO-field is turned off at 18.5 ps. The two DWs carry $v > v_e$ but the attractive potential after the elastic collision recombine them in the simulation time window. (**d**) Phase diagram of the different outcomes from a collision event in terms of the amplitude of the SO-field and its duration. Green dots represent inelastic collisions at $v > v_{crit}$ when the SO-field is still on at the collision instance. Orange dots correspond to elastic conditions. Blue dots consist of a first elastic collision followed by an inelastic collision. Red dots represent inelastic collisions at $v < v_{crit}$ when the SO-field is absent at the collision moment. Black dots correspond to a situation where the SO-field is turned of so early that during the computational time window, no collision is observed.

where the coefficient ξ depends on material parameters only but note that due to the Lorentz invariance the AF DW width on the r.h.s. of this equation is velocity- dependent. Solving explicitly for the escape velocity as a function of SO-field gives:

$$v_e(H_{so}) = \frac{\xi \Delta_0 [1 - \Lambda(H_{so})]^{1/2}}{\left[1 + \frac{\xi^2}{v_m^2} \Lambda(H_{so}) \Delta_0^2\right]^{1/2}}. \tag{5}$$

where

$$\Lambda(H_{so}) = v_m^2 \frac{(\gamma H_{so} \Delta_0)^2}{(\alpha v_m)^2 + (\gamma H_{so} \Delta_0)^2}. \tag{6}$$

The above equation tells us that the escape velocity depends upon the SO-field and implicitly on the distance the particle needs to *tunnel* through.

In the following, we present our numerical work which corroborates our conclusions. Figure 3 shows the DW speed as a function of the SO-field obtained by our theoretical prediction Eq. (5) (blue line) together with the DW velocity (red line) and its width (orange line) versus SO-field. The last two quantities follow Lorentz increase/contraction. It can be observed that for SO-fields larger than $H_{cr} \simeq 20$ mT the actual velocity of the DW is larger than the critical escape velocity and therefore an elastic collision is observed (Orange filled region). On the contrary for fields smaller than H_{cr}, the velocity of the DW is smaller than the escape velocity resulting in both particles being trapped by the attractive potential provided by the other particle. In such a case, an inelastic collision takes place resulting in a DW recombination (purple region). Note that the escape velocity decreases with the increase of the SO field while the DW velocity increases. The intersection is possible for large velocities only which also favors rapid tunneling and short leaving time of the bound state, providing non-decay conditions. The critical velocity is in a good agreement with what is observed by direct simulations in Fig. 2.

Hence, both our direct modelling and analytical approach demonstrate that the SO-field strength and duration can be tuned the way that the collision of AF DWs with opposite topological charges would result either in elastic or inelastic outcome. This result can be beneficial for building AF-based future electronic devices for example for constructing possible circuit outputs. In the following we present a possible scenario for two logical operations.

Outlook: proposal for NOT and XOR gates

Spintronic devices offer a high functionality such as: non-volatile memory, fast operational speeds, well developed routes for writing and reading data, stochastic and even chaotic dynamics for a wide range of magnetic materials[39–42]. Moreover, there have been multiple proposals for logic networks, where the non-volatile nature of the magnetic encoded data would allow for the memory and processing to occur at the same medium. Specifically, topological magnetic solitons (and consequently AF DWs) could be useful for preserving information because of their topological protection. The so-called billiard ball model[43,44] showed that given a sufficient number of particles, which can collide elastically, any sort of computation can be achieved. Of particular interest is whether such solitons could emulate logic gates. In order to achieve this, a classification is necessary from the evolution space as it cannot be inferred from a local topological rule. As the energy of both logic AF DWs is the same while moving, the logic levels are distinguished by the twofold value of the associated WN in the computing region. Interestingly, this system emulates the so-called conservative logic[45], which conserves the physical quantities in which the digital signal is encoded. In particular the WN would be a conserved Boolean quantity. The binary values 1 and 0 are represented by the winding number of a given AF DW. As we previously discussed, the DW winding number is switched after an elastic collision event giving raise to a NOT-gate.

However, in order to implement universal logic gates such as XOR-gates one requires to add further complexity to the system. Figure 4 shows a schematic proposal for a XOR-gate which consists of two free DWs with opposite WNs and a pinned DW with an arbitrary WN. One input to the XOR is associated to magnetic texture's central spin polarization, $m_x > 0$ and $m_x < 0$ which correspond to logic values 1 and 0 respectively. The second input concerns the SO-field value. The logic value 1 is associated with the critical SO-field, $H > H_{\text{crit}}$ at which a proliferation of DW-pairs with overall WN=0 is observed[13]. The logic value 0 corresponds to $H < H_{\text{crit}}$, see Fig. 4, panels a and b. The output signal after the second collision (see Fig. 4 panels c–f) corresponds to binary values 1 and 0 characterised by the presence or absence of a DW in the output region. Figure 4c shows that after an elastic collision among the two free DWs the resulting DW is accelerated (SO-field increases, see Fig. 4a) towards the pinned DW where another elastic collision occurs due to the fact that both DWs have the same WN. The output of this collision is therefore a texture which represents logic value 1. Figure 4d represents once again first an elastic collision among two DWs with opposite WN but, this time after the collision, the SO-field is increased
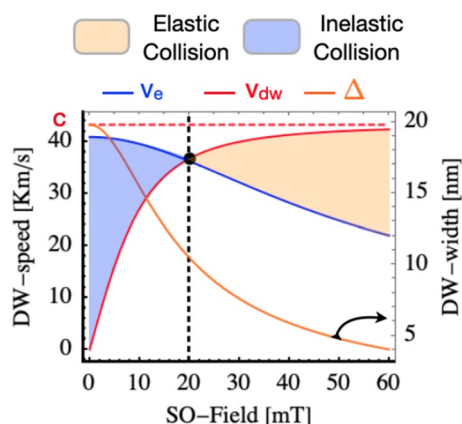
Figure 3. DW velocity, v_{dw}, DW width, Δ, and escape velocity, v_{dw}, a as a function of the SO-field. Red dashed line represents the maximum speed velocity extracted from the dispersion relation, ~ 43.3 km/s. For SO-fields larger than the H_c 20 mT, the DW velocity induced by the SO-field is larger than the escape velocity (light orange region). However, for SO-fields lower than H_c, the DW can not escape from the attractive potential provided by the other DW as the $v_{\text{dw}} < v_e$ (light blue region).
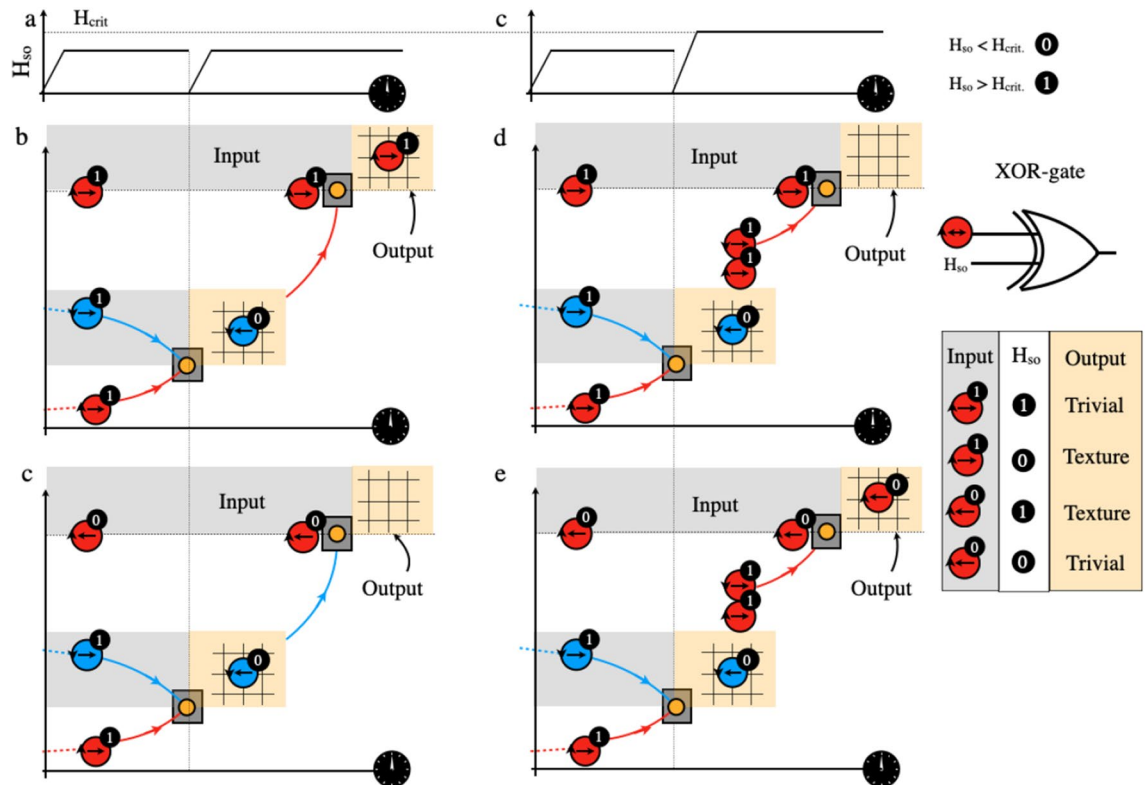
Figure 4. (**a**) Temporal evolution of the spin–orbit field, H_{so}. (**b**) Temporal evolution of the spin–orbit field, H_{so}, which will results for a different output when $H_{so} > H_{crit}$. (**c**) shows an elastic collision among two free domain walls (DWs) with opposite winding number, followed by a second elastic collision with a pinned DW in the output region represented in orange. (**d**) shows an elastic collision among two free DWs with opposite winding number, followed by the nucleation of another domain wall, with overall WN=0. A second inelastic collision occurs among one of the nucleated DWs and a pinned DW. (**e**) Same scenario as in panel **c** but with a pinned DW with opposite polarization. (**f**) Same scenario as in panel **d** but with a pinned DW with opposite polarization.

above a value larger than H_{crit} resulting in the nucleation of a DW pair with opposite WN. It is known that there is a specific arrangement of the two generated DWs[13]. The one further away from the initial DW has an opposite to it WN. This DW is then accelerated towards the pinned DW but this time, both DWs suffer an inelastic collision and annihilate each other representing a logic value 0. Figure 4e represents the same situation as in Fig. 4c but now the pinned layer has opposite polarization than the one in Fig. 4c. In this situation, under the action of the SO-field represented (see Fig. 4a), the second collision is inelastic as both DWs have opposite WN resulting in a 0 in the logic output. Figure 4f, shows the same situation as in Fig. 4d but with opposite polarization for the pinned layer and same temporal evolution of the SO-field as in panel b. Once again, as the spin–orbit field is lager than H_{crit} after the first collision a nucleation event occurs. The generated DW this time has the same WN as the pinned one and the collision is inelastic. Therefore, the output region contains now a magnetic texture. If we associate the presence or absence of a magnetic texture by binary values 1 and 0 respectively, we obtain the standard XOR-gate logic table, see Fig. 4g. We emphasize that the reason why the XOR-gate can be created is due to the conservation of overall WN even when multiple AF DWs are generated. Hence this proposal is related to the so-called conservative logic[45] which is characterized by the conservation of certain physical quantities. In our case, the overall topological winding number is associated to the spin space.

Discussion

In this work we have shown that antiferromagnetic DWs moving at relativistic speed can behave as solitons even in the presence of damping. We have provided a phase diagram for the output of two DWs collisions in terms of the SO-field (current) duration and strength. Importantly, the classification of these scattering events cannot be inferred from a local topological rule as we show that the collision of AF DWs with opposite topological charges can produce a variety of different scenarios, including elastic and inelastic outcomes. So far, studies in ferromagnets have shown that DWs with opposite winding numbers always recombine. Those studies kept the external magnetic field turned on preventing DWs to separate from each other due to the Zeeman energy penalty.

However, a more fundamental reason why DWs in ferromagnets do not show elastic collisions under normal conditions is the fact they cannot move at speeds required to escape the interaction potential. This is due to the fact that unless extreme conditions are meet concerning the biaxial anisotropy values[46], the DW always enter in the so-called Walker Breakdown. For instance, for parameters extracted from[36], and typical speed of 100 m/s the corresponding DW kinetic energy is about 5 orders of magnitude lower than the strength of the attractive interaction potential, preventing an elastic collision to occur. Estimations show that in ferromagnets the required speed to have elastic collision would be several orders of magnitude larger than the maximum group velocities of the magnons ('effective speed of light'). Thus, even if the Walker breakdown could be prevented, this becomes impossible to achieve. Therefore, the ultimate reason for the elastic collision is that antiferromagnetic DWs obey relativistic dynamics. Thus, this soliton character of DWs seems to be reserved only for antiferromagnets irrespective on the overall winding number of the system.

Combining soliton intrinsic stability with topological protection provides an indestructible approach to transmit information or store energy even when collisions occur. Due to the fact that AF DWs can show elastic collision behavior while preserving the overall winding number, they can act as the building block for soliton-based unconventional computing[1,2]. The application of current effectively "charge" them with relativistic exchange energy[14] which can be transported on a long distance and be released by inelastic collisions. As shown, logic conservative computation performed by AF DWs does not required any hard-wiring as in conventional computing. Instead, the *wiring* is provided by the spin medium in the sense that it does not need any fixed hardware structures. Moreover, spintronic-based soliton computing would share the advantages of several schemes such as neuromorphic and reservoir computing[47,48] since the memory and computation are located in the same processing unit. Comparatively to these applications, antiferromagnetic domain walls are smaller (with sizes down to several nanometers) and can reach velocities circa 35 km/s (35 nm/ps) in timescale of 5-10 ps offering faster clocking times. Multiple additional advantages could be envisaged: the AFM-DW based computing could be parallel (not-sequential), energy-efficient and have large quality factor (see more details in Supplementary Material). Thus, topological solitons in AF materials could be a good alternative for high speed and dense integrated circuits in technologies based on the application of conservative logic principles of solitons.

Methods

We consider a magnetic stripe located in xy-plane with a long dimension in x-direction. The domain wall dynamics are solved on a spin-atomic cell structure of Mn_2Au. Mn_2Au lattice cell is composed of totally 10 Mn-sites. In our convection, 4 occupied basal-planes are located in the xy plane with anti-parallel magnetisation orientations along z direction. Upon passing a current along the x-direction, the alternating polarisation of spin-accumulation takes place which gives rise to the corresponding staggered magnetic field, $\mathbf{H}_{so}$ acting locally on each atomic site and oriented along ±y-direction. The computational domain is 7500 cells long, one cell wide with periodic boundaries along the stripe width (y-direction). The time evolution of a unit vector spin at site i, $\mathbf{s}_i$, is simulated by solving the Landau-Lifshitz-Gilbert equation:

$$\frac{d\mathbf{s}_i}{dt} = -\gamma\,\mathbf{s}_i \times \mathbf{H}_i^{\text{eff}} - \gamma\alpha\,\mathbf{s}_i \times \left(\mathbf{s}_i \times \mathbf{H}_i^{\text{eff}}\right), \tag{7}$$

where α is the Gilbert damping set here to 0.001 and $\mathbf{H}_i^{\text{eff}}$ is the effective field resulting from all of the interaction energies. The energies include the three exchange interactions (two antiferromagnetic and one ferromagnetic), magneto crystalline energy contributions and the SO-field. The total energy, E is given by

$$E = -2\sum_{\langle i<j \rangle} J_{ij}\mathbf{s}_i \cdot \mathbf{s}_j - K_{2\perp}\sum_i \left(\mathbf{s}_i \cdot \hat{\mathbf{z}}\right)^2 - K_{2\parallel}\sum_i \left(\mathbf{s}_i \cdot \hat{\mathbf{y}}\right)^2$$
$$- \frac{K_{4\perp}}{2}\sum_i \left(\mathbf{s}_i \cdot \hat{\mathbf{z}}\right)^4 - \frac{K_{4\parallel}}{2}\sum_i \left[\left(\mathbf{s}_i \cdot \hat{\mathbf{u}}_1\right)^4 + \left(\mathbf{s}_i \cdot \hat{\mathbf{u}}_2\right)^4\right] - \mu_0\mu_s\sum_i \mathbf{s}_i \cdot \mathbf{H}_i^{\text{eff}}. \tag{8}$$

The first term on the right-hand side is the exchange energy where J_{ij} is the exchange coefficient along the considered bonds. The second and third terms are the uniaxial hard and easy anisotropies of strengths $K_{2\perp}$ and $K_{2\parallel}$, respectively, while the fourth and fifth terms collectively describes tetragonal anisotropy. For the in-plane part of the tetragonal anisotropy, $\mathbf{u}_1$=[110] and $\mathbf{u}_2$=[1$\bar{1}$0]. Finally, μ_0 and μ_s are the magnetic permeability in vacuum and the magnetic moment, respectively. We have used $\mu_s = 4\mu_B$ with μ_B being the Bohr magneton (see Table 1 for material parameters). The tetragonal anisotropy was included for sake of completeness as it is present in this material but its role in the high speed dynamics is negligible due to the weak magnitude of its anisotropy constants.

$J_{i1}k_B^{-1}$[K]	$J_{i2}k_B^{-1}$[K]	$J_{i3}k_B^{-1}$[K]	$K_{2\perp}$[J]	$K_{2\parallel}$[J]	$K_{4\perp}$[J]	$K_{4\parallel}$[J]
−396	−532	115	-1.303×10^{-22}	$7K_{4\parallel}$	$2K_{4\parallel}$	1.855×10^{-25}

Table 1. Literature values for material parameters relevant for modelling the spin dynamics. k_B is Boltzmann's constant.

Data availability
All data are available from the corresponding authors upon request.

References
1. Jakubowski, M. H., Steiglitz, K. & Squier, R. K. When can solitons compute?. *Complex Syst.* **10**, 1–22 (1996).
2. Jakubowski, M. H., Steiglitz, K. & Squier, R. Computing with solitons: A review and prospectus. In *Collision-Based Computing* (Springer, London, 2002).
3. Kivshar, Y. S. & Agrawal, G. *Optical Solitons: From Fibers to Photonic Crystals* (Academic press, 2003).
4. Ablowitz, M. J., Biondini, G. & Ostrovsky, L. A. Optical solitons: Perspectives and applications. *Chaos Interdisc. J. Nonlinear Sci.* **10**, 471–474 (2000).
5. Aitchison, J., Al-Hemyari, K., Ironside, C., Grant, R. & Sibbett, W. Observation of spatial solitons in algaas waveguides. *Electron. Lett.* **20**, 1879–1880 (1992).
6. Trillo, S. *et al.* *Spatial Solitons* Vol. 82 (Springer, 2001).
7. Burger, S. *et al.* Dark solitons in Bose–Einstein condensates. *Phys. Rev. Lett.* **83**, 5198 (1999).
8. Denschlag, J. *et al.* Generating solitons by phase engineering of a Bose–Einstein condensate. *Science* **287**, 97–101 (2000).
9. Busch, T. & Anglin, J. Motion of dark solitons in trapped Bose–Einstein condensates. *Phys. Rev. Lett.* **84**, 2298 (2000).
10. Jungwirth, T., Marti, X., Wadley, P. & Wunderlich, J. Antiferromagnetic spintronics. *Nat. Nanotechnol.* **11**, 231–241 (2016).
11. Baltz, V. *et al.* Antiferromagnetic spintronics. *Rev. Mod. Phys.* **90**, 015005 (2018).
12. Jungwirth, T. *et al.* The multiple directions of antiferromagnetic spintronics. *Nat. Phys.* **14**, 200–203 (2018).
13. Otxoa, R. M. *et al.* Walker-like domain wall breakdown in layered antiferromagnets driven by staggered spin-orbit fields. *Commun. Phys.* **3**, 1–9 (2020).
14. Otxoa, R. M. *et al.* Topologically-mediated energy release by relativistic antiferromagnetic solitons. *Phys. Rev. Res.* **3**, 043069 (2021).
15. Otxoa, R. M., Atxitia, U., Roy, P. E. & Chubykalo-Fesenko, O. Giant localised spin-Peltier effect due to ultrafast domain wall motion in antiferromagnetic metals. *Commun. Phys.* **3**, 31 (2020).
16. Tatara, G., Akosa, C. A. & De Zuazola, R. M. O. Magnon pair emission from a relativistic domain wall in antiferromagnets. *Phys. Rev. Res.* **2**, 043226 (2020).
17. Zvezdin, A. K. Pis' ma zh. eksp. teor. fiz.. *JETP Lett.* **29**, 553 (1979).
18. Pitaevskii, L. & Lifshitz, E. *Statistical physics.* (Butterworth-Heinemann, 1980).
19. Bar'yakhtar, V. G., Ivanov, B. A. & Chetkin, M. V. Dynamics of domain walls in weak ferromagnets. *Soviet Physics Uspekhi* **28**, 563 (1985).
20. Kosevich, A. M., Ivanov, B. A. & Kovalev, A. S. Magnetic solitons. *Phys. Rep.* **194**, 117–238 (1990).
21. Roessler, U. K., Bogdanov, A. & Pfleiderer, C. Spontaneous skyrmion ground states in magnetic metals. *Nature* **442**, 797–801 (2006).
22. Braun, H.-B. Topological effects in nanomagnetism: From superparamagnetism to chiral quantum solitons. *Adv. Phys.* **61**, 1–116 (2012).
23. Manton, N. *Topological Solitons* (Cambridge University Press, 2004).
24. Mougin, A., Cormier, M., Adam, J., Metaxas, P. & Ferré, J. Domain wall mobility, stability and walker breakdown in magnetic nanowires. *EPL Europhys. Lett.* **78**, 57007 (2007).
25. Van Waeyenberge, B. *et al.* Magnetic vortex core reversal by excitation with short bursts of an alternating field. *Nature* **444**, 461–464 (2006).
26. Thomas, L., Hayashi, M., Moriya, R., Rettner, C. & Parkin, S. Topological repulsion between domain walls in magnetic nanowires leading to the formation of bound states. *Nat. Commun.* **3**, 1–7 (2012).
27. Benitez, M. *et al.* Magnetic microscopy and topological stability of homochiral néel domain walls in a pt/co/alox trilayer. *Nat. Commun.* **6**, 1–7 (2015).
28. Purnama, I., Murapaka, C., Lew, W. & Ono, T. Remote driving of multiple magnetic domain walls due to topological interaction. *Appl. Phys. Lett.* **104**, 092414 (2014).
29. Djuhana, D., Piao, H.-G., Yu, S.-C., Oh, S. K. & Kim, D.-H. Magnetic domain wall collision around the walker breakdown in ferromagnetic nanowires. *J. Appl. Phys.* **106**, 103926 (2009).
30. Dong, W., Su, Y., Lei, H. & Hu, J. Manipulation of multiple 360 o domain wall structures and its current-driven motion in a magnetic nanostripe. *AIP Adv.* **5**, 117215 (2015).
31. Yoshimura, Y. *et al.* Soliton-like magnetic domain wall motion induced by the interfacial Dzyaloshinskii–Moriya interaction. *Nat. Phys.* **12**, 157–161 (2016).
32. Togawa, Y. *et al.* Domain nucleation and annihilation in uniformly magnetized state under current pulses in narrow ferromagnetic wires. *Jpn. J. Appl. Phys.* **45**, L1322 (2006).
33. Kunz, A. Field induced domain wall collisions in thin magnetic nanowires. *Appl. Phys. Lett.* **94**, 132502 (2009).
34. Železný, J. *et al.* Relativistic néel-order fields induced by electrical current in antiferromagnets. *Phys. Rev. Lett.* **113**, 157201 (2014).
35. Rama-Eiroa, R. *et al.* Inertial domain wall characterization in layered multisublattice antiferromagnets. *J. Magn. Magn. Mater.* **560**, 169566 (2022).
36. Saitoh, E., Miyajima, H., Yamaoka, T. & Tatara, G. Current-induced resonance and mass determination of a single magnetic domain wall. *Nature* **432**, 203–206 (2004).
37. Feldtkeller, E. Magnetic domain wall dynamics. *Physica Status Solidi (B)* **27**, 161–170 (1968).
38. Tatara, G. & Kohno, H. Theory of current-driven domain wall motion: Spin transfer versus momentum transfer. *Phys. Rev. Lett.* **92**, 086601 (2004).
39. Montoya, E. A. *et al.* Magnetization reversal driven by low dimensional chaos in a nanoscale ferromagnet. *Nat. Commun.* **10**, 1–9 (2019).
40. Alvarez, L. F., Pla, O. & Chubykalo, O. Quasiperiodicity, bistability, and chaos in the Landau–Lifshitz equation. *Phys. Rev. B* **61**, 11613 (2000).
41. Bertotti, G., Serpico, C. & Mayergoyz, I. D. Nonlinear magnetization dynamics under circularly polarized field. *Phys. Rev. Lett.* **86**, 724 (2001).
42. Petit-Watelot, S. *et al.* Commensurability and chaos in magnetic vortex oscillations. *Nat. Phys.* **8**, 682–687 (2012).
43. Durand-Lose, J. Computing Inside the Billiard Ball Model. In *Collision-Based Computing.* (Springer, London, 2002).
44. Adamatzky, A. Collision-based computing in Belousov–Zhabotinsky medium. *Chaos Solitons Fractals* **21**, 1259–1264 (2004).
45. Fredkin, E. & Toffoli, T. Conservative logic. *Int. J. Theor. Phys.* **21**, 219–253 (1982).
46. Rama-Eiroa, R., Otxoa, R. M., Roy, P. E. & Guslienko, K. Y. Steady one-dimensional domain wall motion in biaxial ferromagnets: Mapping of the Landau–Lifshitz equation to the sine-Gordon equation. *Phys. Rev. B* **101**, 094416 (2020).
47. Grollier, J. *et al.* Neuromorphic spintronics. *Nat. Electron.* **3**, 360–370 (2020).
48. Finocchio, G. *et al.* The promise of spintronics for unconventional computing. *J. Magn. Magn. Mater.* **521**, 167506 (2021).

Acknowledgements

Author contributions

R.M.O. conceived the idea. R.M.O. performed numerical simulations. R.M.O., G.T. and O.C.-F. elaborated the theory. All authors analysed and discussed the results. The main manuscript text was written by R.M.O. and O.C.-F. All authors reviewed the manuscript.

Competing interests

The authors declare no competing interests.

Additional information

Supplementary Information The online version contains supplementary material available at https://doi.org/10.1038/s41598-023-47662-z.

Correspondence and requests for materials should be addressed to R.M.O. or O.C.-F.

Reprints and permissions information is available at www.nature.com/reprints.

Publisher's note Springer Nature remains neutral with regard to jurisdictional claims in published maps and institutional affiliations.